

The Nanostructured Origami™ 3D Fabrication and Assembly Process for nanopatterned 3D structures

Hyun Jin In^{*a}, William J. Arora^b, Paul Stellman^a, Sundeep Kumar^a,
Yang Shao-Horn^a, Henry I. Smith^b, and George Barbastathis^a

^aDept. of Mechanical Eng., MIT, 77 Massachusetts Ave., Cambridge, MA, USA 02139-4307;

^bDept. of Electrical Engineering and Computer Science, MIT, 77 Massachusetts Ave.,
Cambridge, MA, USA 02139-4307;

ABSTRACT

Nanostructured Origami™ 3D Fabrication and Assembly Process is a method of manufacturing 3D nanostructured devices using exclusively 2D micro- and nanofabrication techniques. The origami approach consists of first patterning a large 2D membrane and then folding the membrane along predefined regions to obtain the final 3D configuration. We report on the materials, actuation, and modeling aspects of building an origami structure. Experimental results from fabricated devices as well as future applications of the technique are also presented.

Keywords: Three-dimensional (3D) fabrication, microassembly, nanostructured origami, nanotechnology

1. INTRODUCTION

State-of-the-art micro- and nanofabrication techniques can be used to create features down to tens of nanometers via various approaches such as electron beam and x-ray lithography, nanoimprinting, and dip-pen lithography. In most applications where having two-dimensional (2D) features are sufficient, current fabrication techniques are adequately quick, cost effective, and efficient. However, as most micro- and nanofabrication tools and processes are tailored for planar fabrication, non-planar devices and structures can be very difficult to fabricate. For example, a device with multiple, nanopatterned layers needs to go through many tedious deposition, alignment, and patterning steps. In addition, three-dimensional (3D) structures with nanopatterned sidewalls and/or angled surfaces are almost impossible to create using conventional fabrication tools.

The Nanostructured Origami™ 3D Fabrication and Assembly Process [1] is a completely different approach to 3D nanofabrication in which 3D nanosystems are created exclusively using standard, 2D lithography tools. In the first step, commercial and research-grade micro- and nanofabrication tools are used to pattern rigid, 2D membranes with micro- and nanoscale features. Subsequently, these patterned membranes are folded into the desired 3D configuration in a manner similar to the Japanese art of origami, or paper folding. The inclusion of hinges, creases, and actuation mechanisms in the initial 2D patterning step allows these 2D membranes to be automatically folded into almost arbitrary 3D layouts. Furthermore, the use of standard fabrication tools and materials facilitates integration with preexisting processes. The effective use of the 3rd dimension will result in the creation of novel, smart structures with functions previously unattainable in 2D configurations.

In this paper, we report on our progress in various aspects of fabricating nanopatterned 3D structures based on the Nanostructured Origami™ technique. Two variations of the origami fabrication method are described. In the thin film fabrication process, thin membranes are curled into desired, 3D shapes by controlling the residual stress of deposited thin films. Theoretical and modeling aspects of such devices are discussed along with fabrication procedures and results. In the second approach, SU-8, a robust, epoxy-type photoresist, is used as the structural material. The SU-8 segments, connected via metal hinges, are folded using a magnetic force actuation scheme. Because SU-8 is a dielectric and has good optical properties, it is ideal for use in optical applications in the visible wavelength range or when electrical isolation is desired. Fabrication techniques and results for the SU-8 fabrication process are reported along with methods for folding the SU-8 segments. We conclude with origami applications and a summary of our work.

*hji@mit.edu; phone 1 617 258 0649; fax 1 617 258 9346; web.mit.edu/optics/www

2. THIN FILM FABRICATION

The thin film approach to origami fabrication takes advantage of residual stress that can develop in thin film deposition. This built-in stress is translated into a strain that can fold thin films into 3D shapes such as corner cubes, nanotubes, raised bridges, and etc.

2.1 Strain actuated folding theory

Strain actuated folding is achieved by creating a hinge that is a bilayer strip of length l in the region where folding is to take place (Fig. 1). The upper layer of these hinge areas is intentionally deposited with as much residual stress as possible. This intrinsic stress creates a strain through the thickness of the bilayer. When the bilayer is released from the substrate, it curls to fold the structure.

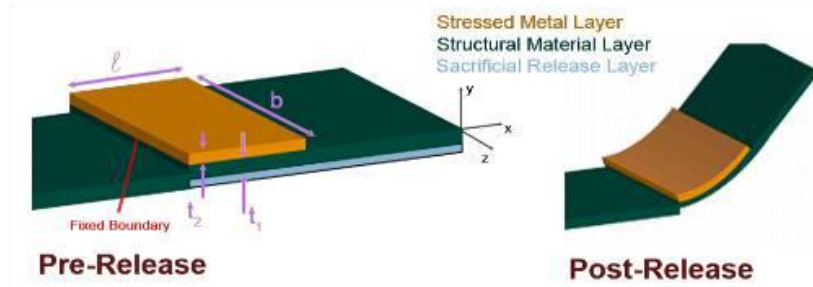


Figure 1: Schematic of the strain actuated folding method. The structural layer (bottom, green) is referred to as layer 1. The stress metal layer (top, orange) is referred to as layer 2. The interface between the two layers is at $y=0$.

If the curling radius of the hinge is known beforehand, the hinge length can be adjusted to control the angle of the fold. Therefore, we have modeled the curling of a bilayer thin plate structure to derive an expression for ρ , the radius of curvature. This formula was also derived by Nikishkov [2]. Other models of this problem can be found in Cybulski [3], Vaccaro [4], and Grundmann [5]. Our model is shown in Figure 1. Layer i has elastic modulus E_i , poisson ratio ν_i , and initial stress σ^i . Layer 2 is a stressed metal deposited by evaporation and we assume it is in a state of plane stress. Additionally, we assume that the rectangular geometry and fixed boundary conditions constrain the folding about the z axis and prevent any strain along the z axis. These assumptions are expressed by

$$\sigma_y = 0, \quad (1)$$

$$\varepsilon_z = 0. \quad (2)$$

We use elastic theory (Hooke's law) to model the strain in the structure as

$$\varepsilon_x = \frac{\sigma_x}{E} - \nu \frac{\sigma_z}{E}, \quad (3)$$

$$\varepsilon_z = \frac{\sigma_z}{E} - \nu \frac{\sigma_x}{E}. \quad (4)$$

Solving (3) and (4) together with assumptions (1) and (2) we obtain

$$\sigma_x = \frac{E}{1-\nu^2} \varepsilon_x. \quad (5)$$

Therefore, we use a modified elastic modulus constant,

$$E_i' = \frac{E_i}{1-\nu^2}; i = 1, 2, \quad (6)$$

and can now calculate the initial strain

$$\varepsilon^i(y) = \begin{cases} \frac{\sigma^{(1)}}{E_1'}, & y < 0 \\ \frac{\sigma^{(2)}}{E_2'}, & y > 0 \end{cases} \quad (7)$$

From simple beam theory, we know that a radial bend of curvature k will produce a linear strain gradient through the thickness, plus a possible constant strain ε^o attributed to a residue of initial strain

$$\varepsilon_x(y) = \varepsilon^o + ky. \quad (8)$$

We can also express the strain in the x direction as

$$\varepsilon_x(y) = \frac{\sigma_x(y)}{E'(y)} + \varepsilon^i(y), \quad (9)$$

where ε^i are the intrinsic strains in both layers from their deposition, respectively. E' is a function of y because of the material interface at $y=0$. Combining (8) and (9) yields the stress

$$\sigma_x(y) = E'(y) \cdot [\varepsilon^o + ky - \varepsilon^i(y)] \quad (10)$$

After the bilayer has been released and curled, it is in a state of static equilibrium. We describe this with force and moment balance equations

$$0 = F_x = b \cdot \int_{-t_1}^{t_2} \sigma_x(y) dy, \quad (11)$$

$$0 = M_z = b \cdot \int_{-t_1}^{t_2} y \cdot \sigma_x(y) dy. \quad (12)$$

Solving (11) and (12) simultaneously yields the radius of curvature

$$\rho = \frac{1}{k} = \frac{E_1'^2 t_1^4 + E_2'^2 t_2^4 + 2E_1'E_2't_1t_2(2t_1^2 + 2t_2^2 + 3t_1t_2)}{6E_1'E_2't_1t_2(t_1 + t_2) \cdot \varepsilon_{tot}^i}. \quad (13)$$

The curling radius is thus a function of material properties, thickness and initial strain. The two materials of interest for our structural layer are silicon nitride and silicon dioxide. They can be deposited without residual stress and are often used in optical MEMS. We have used chromium for our stressed metal layer because it can be evaporated with more than 2 GPa of intrinsic tensile stress, and because it is highly etch selective. In our experiments, we show results using silicon nitride and chromium bilayers. Using these material properties ($E_1'=313$ GPa, $E_2'=167$ GPa) and fixing the thickness of the silicon nitride layer to 200nm, the dependence of the radius of curvature on chrome layer thickness is shown in Fig. 2.

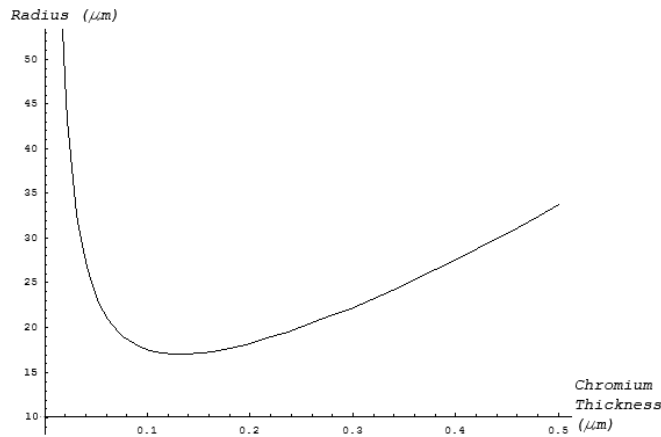


Figure 2: Radius of curvature vs. thickness of the stressed metal layer, both in microns.

We would like to minimize the radius to make the hinges as small as possible. Fig. 2 shows that t_2 should be between 110-150nm for our chosen material parameters.

We have also constructed a finite element model (FEM) of the same problem. The model exhibits large elongation along the x axis which is not predicted by theory or seen in experiment. We are working to improve the model by incorporating thin film material properties to account for microscopic defects and other limitations of continuum theory. Fig. 3(b) shows that stress profile through the thickness of the beam is linear and maximal at the material interface. This agrees with our beam bending theory. The estimated radius of curvature of the FEM is within 20 percent of the measured and theoretical values. This discrepancy will be accounted for when we use more sophisticated material models and analysis techniques.



Figure 3: (a) FEM showing the post-release behavior of a stressed metal bilayer hinge; (b) Stress profile through the thickness of the hinge.

2.2 Strain folding procedure

Our experimental procedure is shown in Fig. 4. We have chosen chromium to be the stressed metal layer because it can be vacuum evaporated with nearly 3 GPa of tensile stress. The choice of silicon nitride as the structural layer is justified because it can be LPCVD deposited with nearly zero stress. Finally, silicon dioxide is best as release layer because it can be etched away without affecting the silicon nitride and chromium. (In our experimental trials, we found that the etch selectivity between silicon dioxide and silicon nitride was not sufficient; this is discussed below).

Release islands are first defined so that during the release step, the devices only are released from the wafer. There are two considerations in choosing a release layer thickness. First, it must be approximately equal to half the thickness or less of the structural layer to avoid creating a large step discontinuity in the structural thin film. Second, it must be thick enough to avoid significant stiction problems between the silicon wafer substrate and the released structural membrane. In our experiments with silicon dioxide as the release layer we have used a release layer thickness between 20 - 100 nm. Silicon dioxide was grown in a wet furnace and the release islands were defined with a positive photoresist etch mask in a buffered HF wet etch.

Silicon nitride is deposited on the patterned silicon dioxide in an LPCVD process. We have used 200-400 nm thick silicon nitride. To obtain the smallest radius of curvature, the structural layer at the hinge area should be as thin as possible. With a 200 nm thick silicon nitride layer it is possible to obtain an 18 μm radius fold. Although a thinner layer could have been used, it would have made the extending silicon nitride device membrane structurally fragile. (To obtain a smaller radius of curvature, the mask used to pattern the stressed metal hinges in step three could also be used to thin the structural layer at the hinge area. Although in these experiments we did not try this, this is how one would fold thicker membranes.) The silicon nitride is patterned as shown in step 2 using a CF_4 gas plasma reactive ion etch with a 25 nm thick nickel hard mask.

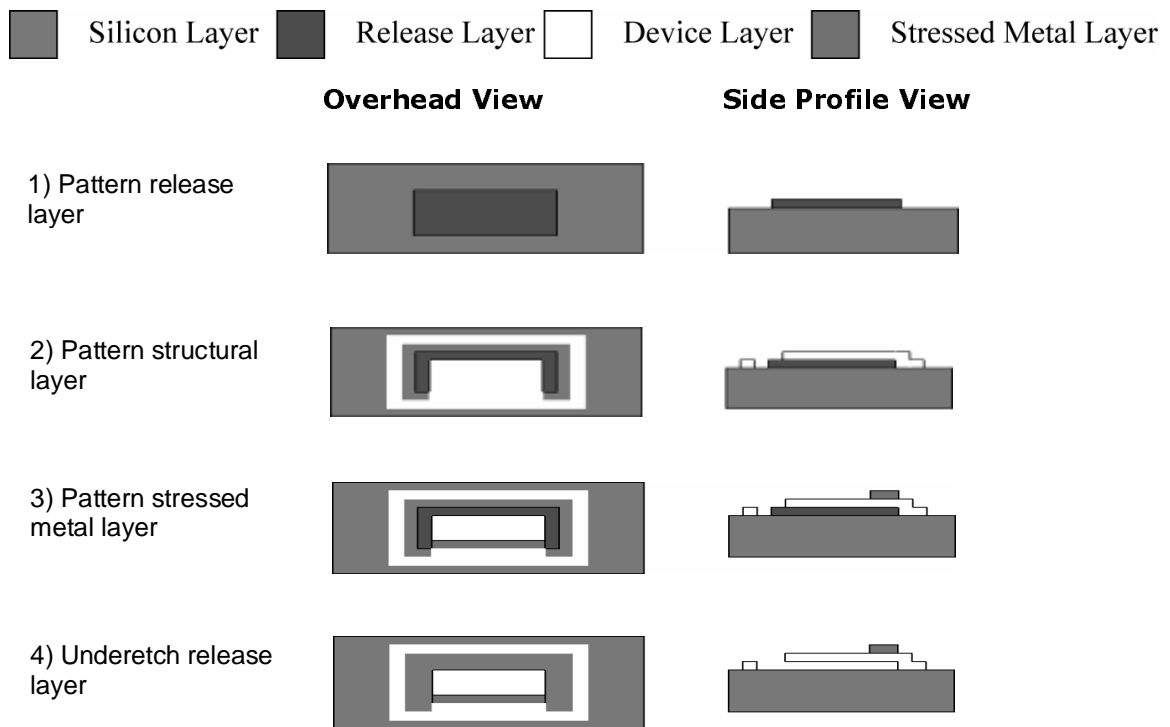


Fig. 4: Processing steps for strain actuated folding structure.

The length and width of the hinge area were determined from (13). Knowing prior to fabrication the thicknesses of silicon nitride and chromium used at the hinges, we calculated the resultant folding curvature and thus the hinge length (see Fig. 1) required to fold to a specific angle. The width of the hinge area is always at least four times the length of the hinge area. This is done to ensure that the hinge will fold uniaxially along the z-axis. The stress in the deposited chromium is uniform in the x-z plane; therefore the geometry of the hinge must be chosen to force the hinge to prefer to curl about the z-axis. The lateral dimensions of the hinges in our experiments ranged from 10 x 40 μm to 100 x 400 μm (length \times width).

The stressed chromium metal is deposited by evaporation. We found that when the chromium was wet patterned to the hinge areas, it lost most of its tensile stress. Therefore, the chromium deposition should be done as a liftoff and always as the final step before the release process. Therefore, any device fabrication on the device area of the structural layer should be done before the stressed metal deposition and patterning step (step three in Fig. 3). In our experiments, we deposited 100 nm of chromium onto the silicon nitride and patterned it via a lift-off process.

Finally, the silicon dioxide release layer was underetched in buffered HF. The etch selectivity required to release the smallest silicon nitride membrane was approximately 1000:1 (this would have thinned the silicon nitride membrane by 10% or 20 nm). However, the etch selectivity was observed to be less than 100:1 and most of the silicon nitride was completely etched away before the silicon dioxide could be underetched. Although other etch methods, in particular vapor HF etching, could have been experimented with, in order to achieve good results we simplified the process and eliminated the release layer. The devices were released by directly underetching the silicon with an anisotropic KOH etch, exactly the same as is often used to release cantilevers in MEMS work.

2.3 Strain folding materials

The choice of material to be folded in this technique is not limited to silicon nitride. There are two requirements that limit structural material selection: it must be perfectly etch selective against the release layer material, and it must be stress free and structurally stable. The release layer material also must maintain two requirements: it should be perfectly etch selective against both the structural and stress layer, and should allow the deposition of the structural material on it. In addition to the work presented with chromium, silicon nitride and silicon dioxide (as the stress, structural and release layers respectively), we have also experimented with chromium, silicon dioxide and copper. Although these materials meet the above requirements in theory, in practice we have not been able to get silicon dioxide to adhere well to the release layer. We plan to solve this problem by using CVD silicon dioxide instead of evaporated silicon dioxide in our next experiment. Other material choices that would work but we have not explored yet are: chromium, silicon (single or poly-crystalline) and silicon dioxide.

2.4 Strain folding results

Our experimental results demonstrate controllable folding of thin films using stressed metal hinges. Fig. 5 shows how increasing the length of the hinge changes the angle of the fold.

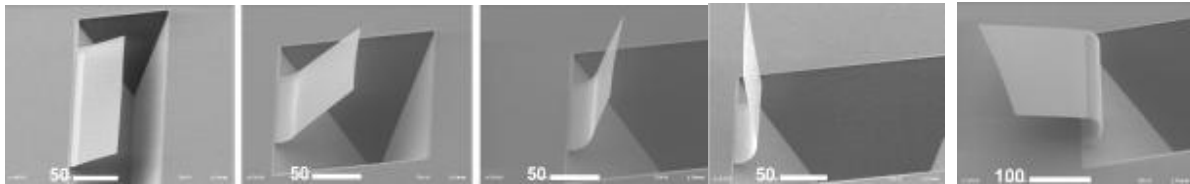


Figure 5: Folding angle can be controlled by varying the length of the stressed metal hinge. Scale markers are in micro-meters.

Fig. 6 shows that the entire device may have multiple hinges. The length of the device in Fig. 6 is approximately 400 μm long and there is no evidence of mechanical failure due to size.

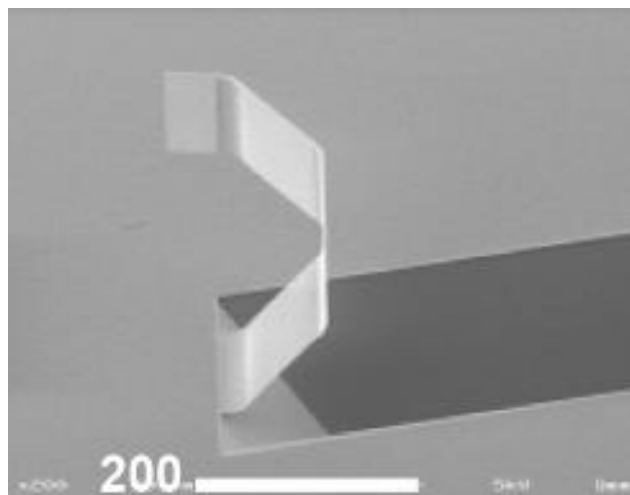


Figure 6: A four hinge device.

Of the approximately five hundred origami devices patterned on our wafer, only about thirty folded as we expected. Several problems contributed to this low yield of roughly 6%. Stiction was the biggest problem. Even though a deep trench, in many cases about 100 μm deep, was etched into the silicon, the devices would fluctuate during the KOH etch and stick to the bottom of the trench. The stiction force is greater than the bending force generated by the hinges which left many devices sunk in the trenches. On the other hand, devices that were designed to fold 180° such as that shown in Fig. 5.5., tended to stick to the wafer after folding out of the trench (Fig. 7).

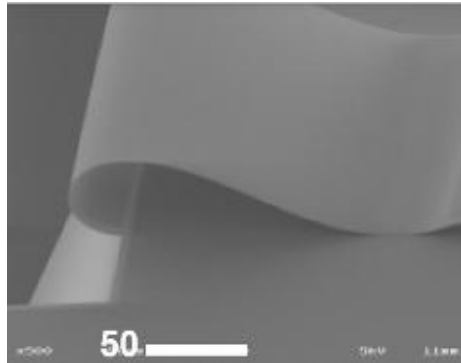


Figure 7: Stiction between folded device and wafer.

The second major problem was due to the anisotropic nature of the KOH underetch. The KOH etches in diagonally from the convex corners of the device. The device membranes are released first, and towards the end of the etch the stressed hinges are released. Because the hinges are released in this diagonal fashion, they begin curling from the sides. In many devices, this created a predictable triangular stress fracture, as shown in figure 8.

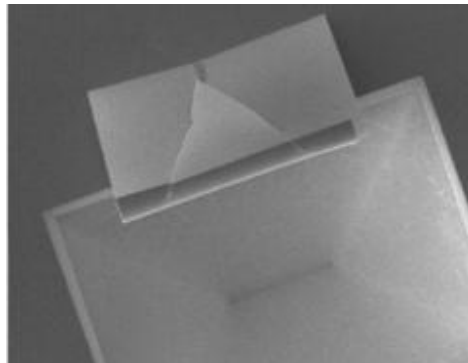


Figure 8: Triangular stress fracture observed in many devices.

In our future experiments, we plan to address these two causes of failure by incorporating the release layer described in Fig. 5 (which can be etched isotropically) and by using a dry release etch (such as HF vapor) or a supercritical drier to eliminate surface tension forces while drying the wet-released devices.

3. SU-8 FABRICATION

The very first origami prototypes [1] were fabricated on silicon-on-insulator (SOI) wafers. The 5 μm thick device layer of the SOI wafer served as the rigid, origami membrane and was released by etching away the underlying oxide layer. In order to reduce the complexity of the silicon fabrication process and avoid having to use costly SOI wafers, a simpler process involving octafunctional epoxidized novalac, or SU-8, was developed. SU-8 is a robust, epoxy-like photoresist used commonly as a structural material in MEMS applications. For the Nanostructured Origami™ process, additional advantages of the SU-8 process include optical transparency, high aspect ratio, wide range of achievable thicknesses (from 1 μm to several millimeters), and the ability to be patterned on both sides.

3.1 SU-8 fabrication process

The basic process flow for the SU-8 fabrication method is shown in Fig. 9. Starting with a (100) silicon wafer, a KOH etch step defined patterns (inverted pyramid-shaped trenches of varying sizes) into the substrate. A layer of gold was then deposited and patterned to define the hinges. Subsequently, SU-8 was coated and patterned to serve as the structural layer for the origami segments. The patterns defined in the previous KOH etch step acted as a mold for patterning the bottom side of the SU-8. In the final release step, XeF₂ gas was used to isotropically etch away the underlying silicon thereby releasing the entire structure. Fig. 10 shows a 3-layer SU-8 device after fabrication and folding.

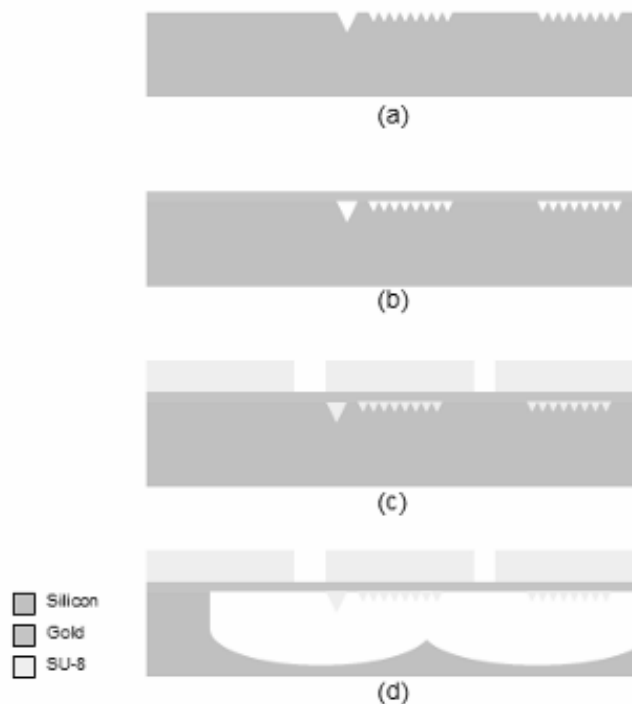


Figure 9: Process flow for SU-8 fabrication. (a) KOH etch defines patterns on the substrate. (b) Deposition and patterning of gold layer for hinges and wires. (c) Coating and patterning of SU-8 layer. (d) XeF₂ release.

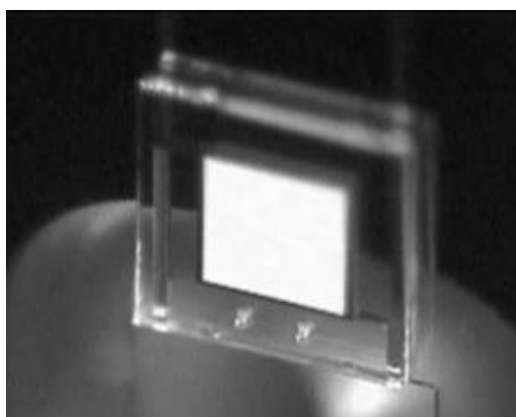


Figure 10: 3-layer SU-8 device after complete assembly.

3.2 Actuation methods for the SU-8 process

In order to enable batch fabrication of the origami devices, an automated, parallel folding scheme is required. For this purpose, the strain induced actuation method (discussed in Section 2) and the magnetic force actuation method were developed and successfully used to fold released devices without the need for manual folding.

The magnetic force actuation method takes advantage of Lorentz law to fold the structures. When an external magnetic field parallel to the substrate is applied to a section of the device with a current loop running through it (provided by the gold wires), an upward force is generated by Lorentz law as shown in Fig. 11. By controlling the current to individual segments, the amount of force applied to each folding membrane, and thus its motion, can be precisely controlled. With less than 20mA of current, an upward force in the order of 10^{-6} N was achieved [1].

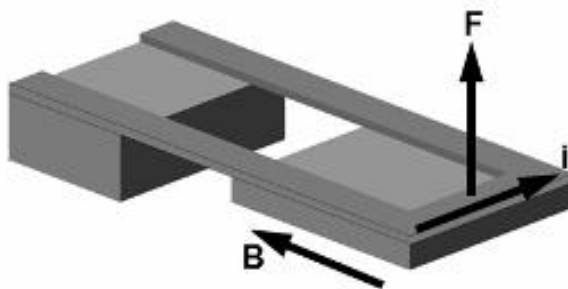


Figure 11: The Lorentz force can be used to raise the desired segment out of plane in the presence of a current loop and a properly oriented magnetic field.

The strain induced actuation method outlined in Section 2 can also be applied to the SU-8 process to automatically fold the membranes upon release. In the current device, the hinges were made of a bilayer of gold and chromium. Because chromium, deposited via electron-beam evaporation, is under high tensile stress, the hinge curls in order to relieve the stress mismatch between layers. By controlling various parameters during deposition, the stress can be engineered to result in a desired radius of curvature [6]. Fig. 12 shows a SU-8 device with gold/chromium bilayer hinges that has popped up out of the substrate upon release due to the residual stress of the chromium.

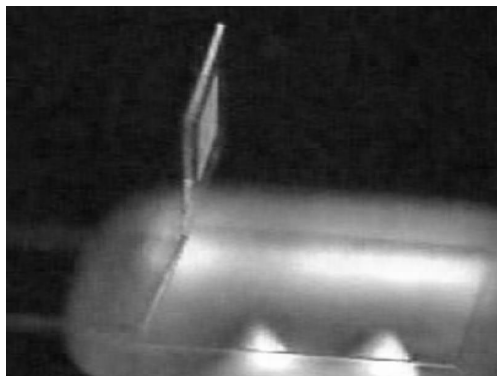


Figure 12: 2-segment SU-8 device with a bilayer hinge made of gold and chromium. The high tensile stress of the chromium has caused the device to pop up from the substrate upon release.

3.3 Spacing and alignment

Alignment precision among the folded layers is crucial in applications such as 3D photonic crystal fabrication, which will be discussed later in Section 4. In this case, nanometer-scale precision must be achieved in both layer-to-layer spacing and lateral alignment of the folded layers. So far, pyramidal alignment features fabricated via anisotropic etching have demonstrated sub-micron spacing and alignment precision [6]. These alignment features, shown in Fig. 13, were created by filling in the anisotropically etched cavities. As the device is folded, square openings on one side fit over the pyramids on the other side. This ensures good lateral alignment as well as layer-to-layer spacing. To push the resolvable level of precision beyond the resolution of the optical microscope, moiré and vernier patterns will be incorporated into future device for improved alignment characterization. Thus far, the pyramidal alignment features have shown $<2\mu\text{m}$ alignment error. This error can be attributed to the photolithography process and was verified by observing the aligned device under a SEM.

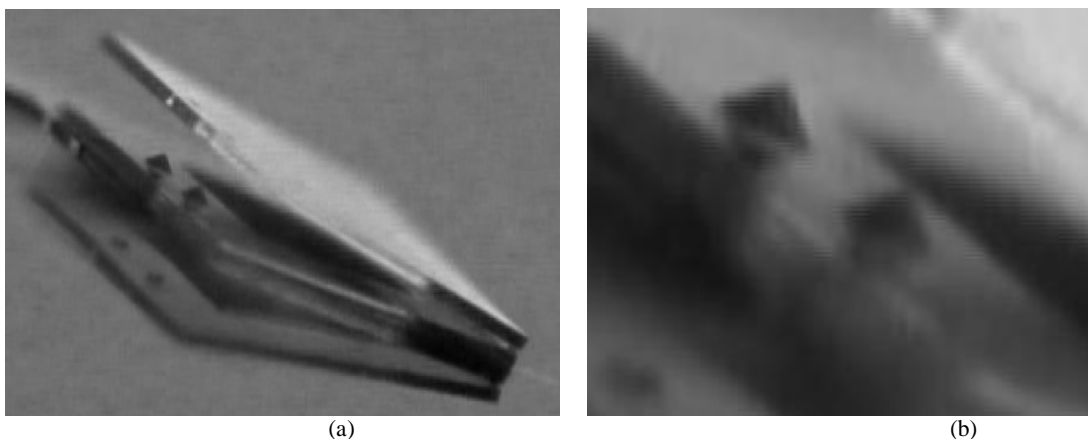


Figure 13: (a) Partially folded SU-8 device with the alignment pyramids. (b) Close-up view of the alignment pyramids.

4. APPLICATIONS

The Nanostructured Origami™ method can be used to fabricate many novel devices that take advantage of the 3rd dimension as well as nanoscale features.

4.1 Supercapacitor

Supercapacitors, also known as electrochemical double-layer capacitors, are emerging as viable alternatives to conventional electrostatic capacitors. Because the supercapacitors use highly porous electrode materials, such as activated carbon, and have atomic-scale charge layer separation distances, higher specific capacitance, and thus higher energy density, is possible. The use of the 3rd dimension allows the creation of more efficient microscale, electrochemical devices, such as multi-layer supercapacitors [7] that have very large electrode areas but a small footprint. For example, an electrochemical device that takes up much space on the chip can be folded to result in a compact, multi-layer, 3D structure (Fig. 14). Nanostructured Origami allows such devices to be formed from a single, micro/nanofabricated layer. In addition, nanoarchitecture can be added to any electrode to increase device performance, for example, in microscale fuel cells. Finally, the Nanostructured Origami™ process is compatible with most standard microfabrication processes and thus allows for an easy integration of electrochemical devices to pre-existing microsystems. These supercapacitors can be used in conjunction with energy harvesters, for example, to provide a constant source of energy for wireless sensors.

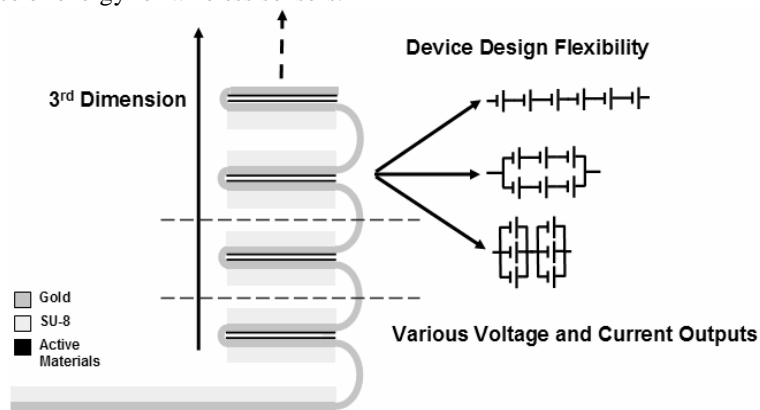


Figure 14: Schematic of a multi-layer supercapacitor with flexible voltage and current outputs.

The finished supercapacitor shown in Figure 15 consists of two SU-8 membranes connected with gold hinges, which also serve to electrically connect the electrodes to the power source. Carbon paint is used as the porous electrode material, and the membranes are folded so that the two electrode surfaces face each other, effectively forming one active cell of the supercapacitor. In the same KOH-etch-and-fill step that was used to form the alignment pyramids, the two electrode areas were patterned with an array of smaller 3 μm ×3 μm pyramids. These pyramids served to increase the total surface area of the electrode area. Preliminary electrochemical testing of the fabricated supercapacitors showed a specific capacitance of approximately 50 farads per gram of activated carbon. This value is comparable to published figures for macroscale supercapacitors with activated carbon electrodes.

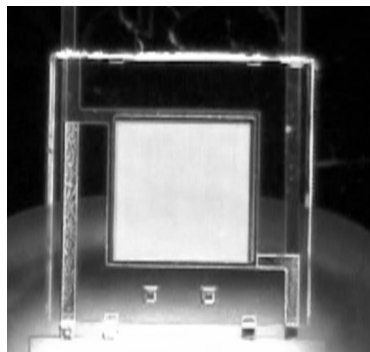


Figure 15: Completely assembled supercapacitor (aligned with alignment pyramids).

4.2 Three-dimensional photonic crystals

Photonics is a promising application domain for the Nanostructured Origami™ process. For example, a 3D photonic crystal can be formed by folding 2D sheets of periodically patterned membranes. The 2D layer can be created via a wide range of fabrication techniques, for example, electron-beam lithography [8], and the folding can be accomplished using the Lorentz force or strain induced methods, as mentioned previously. “Defects,” such as waveguides and cavities, are also formed in straightforward fashion during the 2D patterning step. However, a 3D structure such as the photonic crystal will require each 2D membrane to be folded with an extraordinary level of precision. The alignment techniques used in the Nanostructured Origami™ process will have to be improved significantly to allow alignment precision in the sub-100nm range.

5. CONCLUSION

The Nanostructured Origami™ 3D Fabrication and Assembly Process shows potential for fabrication of novel, nanostructured 3D devices. Unlike other methods for 3D nanofabrication, the Nanostructured Origami™ method relies solely on existing tools and techniques and can thus be integrated more readily into preexisting fabrication processes. Future work will include further development of material selection and fabrication processes, as well as demonstration of applications in the hierarchical assembly of micro- and nanosystems.

REFERENCES

1. S. M. Jurga et al., “Nanostructured Origami,” *Proc. 3rd IEEE Conf. on Nanotechnology*, vol. 2, pp. 220-223, 2003.
2. G. P. Nikishkov, "Curvature estimation for multilayer hinged structures with initial strains," *Journal of Applied Physics*, vol. 94, pp. 5333-5336, 2003.
3. J. Cybulski, "Modeling and Fabrication of Self-Assembling Micron-Scale Rollup Structures," in *Mechanical Engineering*. Cambridge: MIT, 2004, pp. 145.
4. P. O. Vaccaro et al., "Strain-driven self-positioning of micromachined structures," *Applied Physics Letters*, vol. 78, pp. 2852-2854, 2001.
5. M. Grundmann, "Nanoscroll formation from strained layer heterostructures," *Applied Physics Letters*, vol. 83, pp. 2444-2446, 2003.
6. H. J. In et al., “The Nanostructured Origami™ 3D Fabrication and Assembly Process for Nanomanufacturing,” *Proc. 4th IEEE Conf. on Nanotechnology*, pp. 358-360, 2004.
7. Y. Shao-Horn et al., “Origami fabrication of electrochemical device on the micrometer scale,” 204th Meeting of the Electrochemical Society, Orlando, FL, October 2003 (abstract 1279).
8. M. Qi et al., “A three-dimensional optical photonic crystal with designed point defects,” *Nature Magazine*, Vol. 429, 538-542, June 2004.